https://doi.org/10.5194/egusphere-2026-2193
Preprint. Discussion started: 24 April 2026
© Author(s) 2026. CC BY 4.0 License.

Bayesian Joint Retrieval of Soil Moisture from UAV L-Band Radiometry by Integrating RGB-TIR Priors and Footprint-Scale Texture

Zixi Li[1,2], Yan Li[3], Rui Tong[2,4*], Peizhe Cheng[1,2], Fuqiang Tian[1,2,4], Yao Zhuang[4,5]

[1]Department of Hydraulic Engineering, Tsinghua University, Beijing 100084, China

[2]State Key Laboratory of Hydroscience and Engineering, Tsinghua University, Beijing 100084, China

[3]Information Center (Hydrology Monitor and Forecast Center), Ministry of Water Resources, Beijing 100053, China

[4]Fujian Key Laboratory of Severe Weather & Key Laboratory of Straits Severe Weather, China Meteorological Administration, Fuzhou 350008, China

[5]Fujian Meteorological Administration, Fuzhou 350008, China

Correspondence to: Rui Tong (mrtongrui@gmail.com)

Abstract. Accurate field-scale soil moisture is essential for hydrological processes such as infiltration, land–atmosphere exchange, and agricultural water management. UAV-borne L-band radiometry offers a promising intermediate scale between in situ measurements and satellite observations, but retrieval remains ill-posed due to uncertainties in vegetation attenuation, surface temperature, and sub-footprint heterogeneity. This study develops an uncertainty-aware Bayesian retrieval framework that integrates dual-polarized UAV L-band brightness temperature with RGB and thermal infrared information through footprint-consistent priors. Optical fraction cover, thermal state, and texture descriptors are used to constrain vegetation optical depth and its uncertainty at the scale of the radiometric footprint. The method was evaluated over heterogeneous cropland in Pengzhou, China, using independent calibration (4 scenes, ~1.3 ha) and validation datasets (6 scenes, ~3.3 ha). The proposed approach reduced RMSE from ~0.07 to ~0.04 $m^3 m^{-3}$ and largely eliminated the systematic dry bias of the conventional τ–ω inversion. Analysis further shows that sub-footprint heterogeneity primarily increases uncertainty in vegetation attenuation, leading to representation error in soil moisture retrieval. These findings highlight that retrieval performance is fundamentally constrained by observation scale and surface heterogeneity. Overall, the study demonstrates that physically informed multi-source priors can improve both accuracy and interpretability, providing a pathway toward more reliable field-scale soil moisture estimation for hydrological applications.

1. Introduction

Soil moisture regulates energy partitioning, infiltration and runoff processes, and plant water use,

https://doi.org/10.5194/egusphere-2026-2193
Preprint. Discussion started: 24 April 2026
© Author(s) 2026. CC BY 4.0 License.

making it a key state variable in hydrology and land-atmosphere interactions (SU et al., 2014; Li et al., 2022; Wang et al., 2023). Satellite passive microwave missions such as SMOS and SMAP have established L-band radiometry as a physically meaningful approach for large-scale soil moisture monitoring due to its sensitivity to near-surface dielectric properties and reduced influence from vegetation (Kerr et al., 2010; Meyer et al., 2022; Jääskeläinen et al., 2025).

UAV-borne L-band radiometry offers a useful middle scale between plot measurements and satellites. Compared with satellite sensors, drone platforms provide much finer spatial resolution, more flexible acquisition timing, and better control over repeat surveys. The PoLRa platform is one example of a portable L-band system designed for field deployment and UAV integration (Houtz et al., 2020). Recent studies have shown that portable or UAV-compatible L-band radiometers can retrieve meaningful soil moisture under both bare and vegetated conditions, and can be used to test retrieval concepts before transfer to coarser airborne or spaceborne applications (Zhang et al., 2024; Lv et al., 2024; Krishnan et al., 2025; Wang et al., 2024).

However, high spatial resolution does not remove the core inversion difficulty of passive microwave retrieval. L-band brightness temperature still integrates multiple physical controls, including soil dielectric properties, vegetation attenuation, single-scattering albedo, soil surface temperature, and local roughness. In practice, the τ–ω forward model is often calibrated with simplified assumptions, and different combinations of soil moisture and vegetation optical depth can explain similar brightness temperatures. This leads to compensation effects, biased solutions, and uncertainty that is difficult to quantify when the inversion is performed with weak or static priors (Wigneron et al., 2007; Ebtehaj et al., 2019; Zhao et al., 2021; Li et al., 2023; Gibon et al., 2024). Related studies on error propagation in joint microwave retrievals have shown that uncertainty in vegetation terms can directly amplify soil moisture uncertainty, particularly under mixed cover conditions (Feldman et al., 2021; Lu et al., 2025). For field-scale UAV applications, where crop type can change within a short distance, these issues become even more pronounced.

Optical and thermal remote sensing provide a natural complement to L-band radiometry because they describe canopy cover, surface temperature state, and fine-scale spatial organization at a much higher resolution than the microwave footprint. RGB and thermal infrared data cannot replace L-band observations, but they can constrain the physically plausible range of vegetation attenuation

https://doi.org/10.5194/egusphere-2026-2193
Preprint. Discussion started: 24 April 2026
© Author(s) 2026. CC BY 4.0 License.

and indicate whether the microwave footprint is homogeneous or internally mixed. This idea is consistent with broader optical-thermal soil moisture research. Surface temperature and energy-balance approaches can inform root-zone or shallow soil wetness patterns (Alburn et al., 2015; Sahaar et al., 2022; Gao et al., 2022), while drone-based RGB-TIR studies show that thermal and visible cues can improve field-scale soil moisture estimation under crop canopies when local structure is considered explicitly (Li et al., 2022; Shi et al., 2024; Vahidi et al., 2025). Reviews of UAV thermal remote sensing in agriculture also emphasize that thermal imagery becomes more informative when linked to canopy structure and field context rather than interpreted as a standalone moisture proxy (Messina et al., 2020).

Another unsolved issue is the mismatch between the coarse effective support of L-band radiometry and the much finer support of RGB and thermal products. Even at low UAV altitudes, the radiometric footprint remains several meters wide, so the observed brightness temperature represents an area-integrated signal rather than a point measurement (Gruber et al., 2020). When the footprint contains mixed crops, exposed soil, or strong small-scale thermal contrasts, the inversion becomes a nonlinear averaging problem, for which retrieval from averaged brightness temperature is not equivalent to averaging pointwise retrievals. Previous studies have shown that such sub-pixel heterogeneity can distort passive microwave soil moisture retrievals, with errors depending on vegetation and land-cover contrasts within the support area (Burke et al., 2003; Lakhankar et al., 2009; Barrée et al., 2021). In addition, the effective sensing depth of L-band radiometry is itself moisture-dependent, further complicating the relationship between surface measurements and footprint-scale observations (Escorihuela et al., 2010; Shen et al., 2021).

More recent studies have emphasized that addressing scale mismatch and sub-footprint heterogeneity often requires integrating multi-source observations and spatial context information, particularly when bridging coarse microwave signals with high-resolution optical or thermal data (Peng et al., 2023). However, existing retrieval approaches rarely incorporate high-resolution optical-thermal information in a physically consistent manner that matches the microwave footprint and explicitly propagates uncertainty.

This study addresses these challenges by developing an uncertainty-aware Bayesian joint retrieval framework that integrates UAV L-band radiometry with RGB and thermal infrared information,

https://doi.org/10.5194/egusphere-2026-2193
Preprint. Discussion started: 24 April 2026
© Author(s) 2026. CC BY 4.0 License.

explicitly accounting for footprint-scale heterogeneity. The approach has three key advances. First, it introduces physically informed priors, in which RGB-TIR features constrain vegetation optical depth and temperature-related states in a scene-dependent manner. Second, it formulates the retrieval as an uncertainty-aware inversion, enabling joint estimation of soil moisture and its posterior uncertainty. Third, it incorporates footprint-consistent texture integration, ensuring that high-resolution optical and thermal information is aggregated in a manner consistent with the radiometric support.

The framework is evaluated over heterogeneous agricultural fields in the Pengzhou irrigation district, Sichuan Province, using independent calibration and validation datasets. This design allows us to assess not only retrieval accuracy, but also how sub-footprint heterogeneity influences retrieval uncertainty and representation error. In this way, the study provides a physically interpretable pathway for improving field-scale soil moisture estimation and its use in hydrological analysis under heterogeneous land-surface conditions.

2. Materials and Methods

2.1 Study Area and Observation Targets

The study area is located in Pengzhou irrigation district, Sichuan Province, China, on the northwestern margin of the Chengdu Plain (31.0°N, 103.9°E). The region has a humid subtropical monsoon climate, characterized by abundant precipitation, frequent rainfall events during the growing season, and relatively high soil moisture variability. The region is an intensively managed agricultural landscape with relatively flat terrain and mixed land use. The campaign focused on cropland parcels containing wheat, garlic, bare soil, rapeseed, lettuce, and maize. According to field notes and local land-use context, the cultivated soils are dominated by paddy-derived and alluvial agricultural soils that are typical of irrigated plains in the basin margin. The target variable of the study was volumetric surface soil moisture. Scene boundaries and field positions were recorded in campaign geospatial files and were used together with orthomosaics and GPS information for scene registration and validation.

The chosen landscape is suitable for testing the proposed framework because it combines moderate regional uniformity with strong field-scale variability. Adjacent parcels often differ in canopy cover,

https://doi.org/10.5194/egusphere-2026-2193
Preprint. Discussion started: 24 April 2026
© Author(s) 2026. CC BY 4.0 License.

row structure, irrigation history, and exposed soil fraction. This creates local contrasts in vegetation optical depth, surface temperature, and sub-footprint heterogeneity. From a retrieval perspective, these differences challenge any inversion that assumes one homogeneous land surface inside the radiometric support area. From an application perspective, they reflect the actual conditions faced by precision agriculture and smallholder field management in the Chengdu Plain.

2.2 UAV Remote-Sensing System

Two UAV sensing systems were used. The microwave observations were acquired with a DJI Matrice 600 platform carrying the PoLRa v3.1 drone-mounted portable L-band radiometer. PoLRa operates at approximately 1.4 GHz, records dual-polarized brightness temperatures, and is designed for field deployment where a lightweight, portable radiometric package is needed (Houtz et al., 2020). The use of dual polarization is important because the joint response of horizontal and vertical channels improves sensitivity to soil dielectric conditions while still retaining information on vegetation attenuation and scene thermal state.

High-resolution optical and thermal data were acquired with a DJI Mavic 2 Enterprise Advanced. The visible sensor provided RGB imagery for orthomosaics, vegetation fraction proxies, and luminance-based texture analysis, while the thermal sensor provided surface temperature patterns and thermal texture descriptors.

Figure 1. Field deployment of the UAV sensing system, including the (a) DJI Matrice 600 platform carrying the PoLRa v3.1 dual-polarized L-band radiometer and the (b) DJI Mavic 2 Enterprise Advanced used for RGB-TIR survey.

https://doi.org/10.5194/egusphere-2026-2193
Preprint. Discussion started: 24 April 2026
© Author(s) 2026. CC BY 4.0 License.

2.3 Flight Experiment Design and Ground Data Collection

The PoLRa flights were performed at approximately 6 m above ground. The effective microwave support area was approximately 4 m × 7 m based on the radiometric footprint geometry, which later motivated the ellipse-based footprint treatment tested in this paper. The RGB-TIR flights were conducted at approximately 25 m, with 80% forward overlap and 70% side overlap. The resulting products reached an optical ground resolution of about 8 mm and a thermal resolution of roughly 10 cm after mosaicking. These settings provided enough detail to summarize sub-footprint structure while still covering each scene efficiently.

Ground truth soil moisture was measured using a portable TDR probe (HydraGO, Stevens Water Monitoring Systems, USA). At each sampling location, the probe was measured repeatedly and the repeated values were averaged to reduce point noise. The sensing depth was consistent with the shallow near-surface layer that dominates the L-band radiometric response under the observed moisture conditions. The validation labels used in the paper were subsequently spatially clustered to approximately 3 m support in order to stabilize the comparison between point-scale observations and footprint-scale retrievals.

The formal training subset consisted of four scenes (~1.3 ha, a total of 52 calibration points) collected on 03/04 for model calibration. The independent validation subset was based on repeated experiments conducted over two consecutive days (04/04-05/04), during which six scenes were surveyed each day, collectively covering approximately 3.3 ha of agricultural land (57 matched validation points in total). Notably, a rainfall event of approximately 3 mm occurred in the early hours of 05/04; thus, the two validation days represent pre- and post-rainfall conditions, with approximately three days of dry conditions preceding the observations on 04/04. All experimental observations were conducted between 11:00 and 16:00 local time. Representative measurement transects and ground sampling points are shown in Figure 2.

All remote-sensing products were aligned in a common spatial frame using GPS information and manual co-registration checks. The RGB and thermal images were first mosaicked, and the thermal data were converted to temperature layers. The microwave flight lines were corrected for UAV attitude and then interpolated to scene grids for visualization and point matching. Because the support area of the L-band radiometer is larger than the support area of RGB-TIR pixels, the optical

https://doi.org/10.5194/egusphere-2026-2193
Preprint. Discussion started: 24 April 2026
© Author(s) 2026. CC BY 4.0 License.

and thermal variables were summarized inside the assumed microwave footprint rather than sampled at a single pixel. This aggregation step is central to the methodology because it allows the fine-scale imagery to inform the inversion in a way that is consistent with the radiometer's actual sampling geometry.

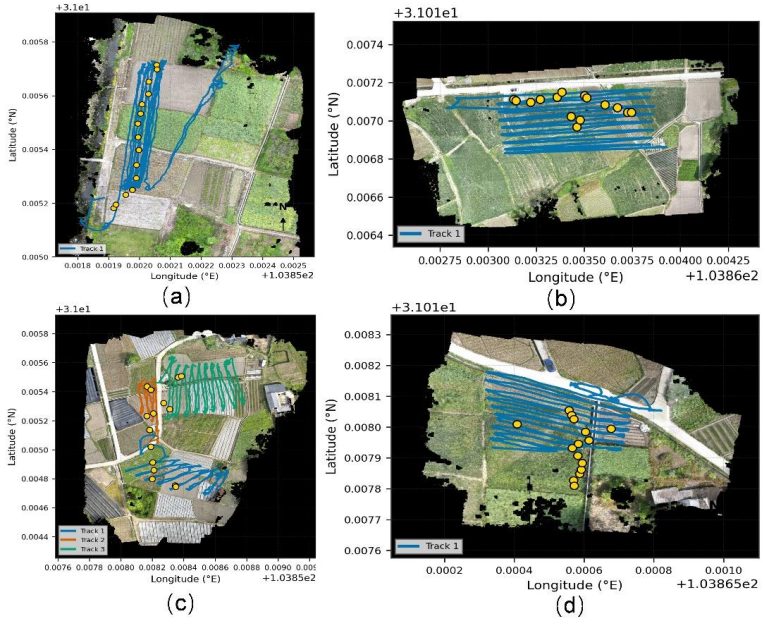

Figure 2. RGB orthomosaic backgrounds with UAV flight trajectories and in situ validation points for representative fields (a-d). Blue lines denote flight tracks and yellow circles denote clustered ground measurements used for calibration or validation.

2.4 Soil Moisture Retrieval Algorithm

The whole framework of the algorithm is shown in Figure 3 (a). The retrieval core is the dual-polarized τ–ω emission model. For polarization p, the brightness temperature can be written as:

$$TB_p = T_g[(1-\omega)(1-\Gamma)(1+r_p\Gamma) + (1-r_p)\Gamma] \quad (1)$$

where Tg is the effective ground or vegetation-soil composite temperature, ω is the single-scattering albedo, rp is the soil reflectivity at polarization p, and Γ = exp(-τ / cos θ) is the canopy transmissivity with optical depth τ and incidence angle θ. The reflectivity term is linked to the complex dielectric constant through the Fresnel equations, while the dielectric constant is related to soil moisture with the Dobson mixing model (Dobson et al., 1985). Equation (1) is standard in L-band passive

https://doi.org/10.5194/egusphere-2026-2193
Preprint. Discussion started: 24 April 2026
© Author(s) 2026. CC BY 4.0 License.

microwave retrieval and forms the physical backbone of both the baseline and the proposed methods (Wigneron et al., 2007).

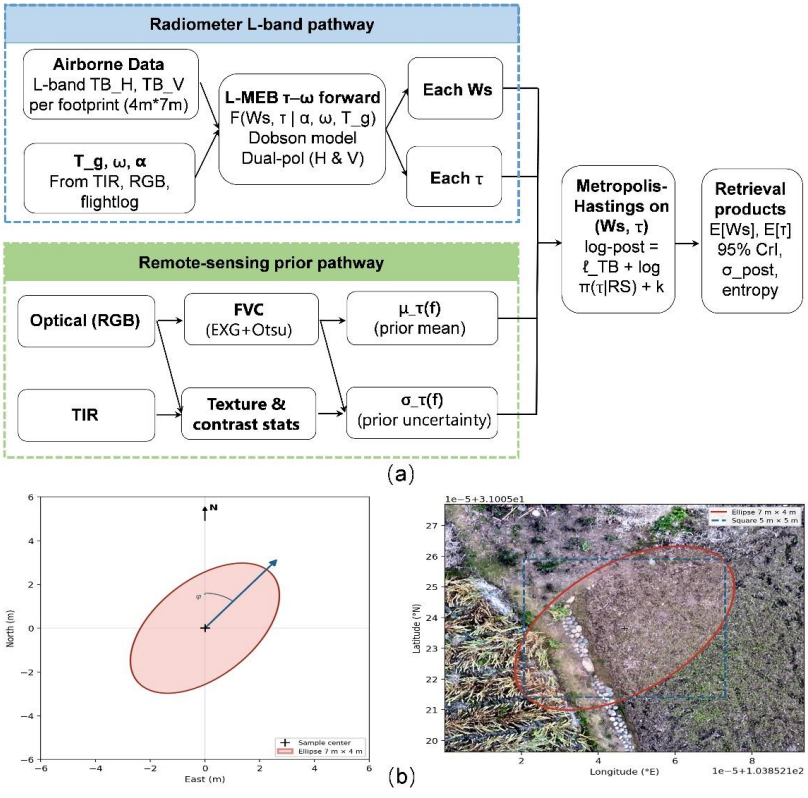

Figure 3. Workflow of the Bayesian joint retrieval. (a) the L-band radiometric pathway and the RGB-TIR prior pathway, and (b) the physically matched 4 × 7 m ellipse footprint used to summarize high-resolution optical and thermal information before Bayesian inversion.

Tg and ω were treated as sample-wise auxiliary states in the forward model. The effective surface temperature Tg was estimated by combining a baseline temperature with a bounded correction informed by thermal observations and optical indicators, including vegetation fraction and footprint-scale heterogeneity. This formulation allows Tg to adapt to local thermal and structural conditions while remaining within physically plausible limits. The single-scattering albedo ω was parameterized as a heterogeneity-dependent term, in which a baseline value was adjusted as a function of a normalized heterogeneity index and constrained within a physically reasonable range. These dynamically estimated Tg and ω values were then used as inputs to the L-MEB τ–ω forward model for likelihood evaluation during the Bayesian retrieval.

https://doi.org/10.5194/egusphere-2026-2193
Preprint. Discussion started: 24 April 2026
© Author(s) 2026. CC BY 4.0 License.

In the baseline inversion, soil moisture Ws and vegetation optical depth τ are solved jointly from the observed TBH and TBV, using fixed or weakly varying ancillary terms and no learned remote prior. This is a practical benchmark because it follows the common strategy of using the microwave observation itself to determine both dielectric and attenuation terms. However, in heterogeneous scenes this joint inversion can become under-constrained. Similar brightness temperatures may be reproduced by a wetter soil with a lower attenuation or by a drier soil with a higher attenuation, especially when independent information on canopy state is limited (Ebtehaj et al., 2019; Zhao et al., 2021).

The proposed framework introduces a Bayesian prior pathway driven by RGB and thermal features. First, RGB orthomosaics were converted into vegetation-sensitive descriptors, including excess green and an Otsu-thresholded fraction vegetation cover term (Meyer and Neto, 2008). Second, both RGB and thermal data were summarized into footprint-scale texture statistics. In practice, the local standard deviation of optical luminance and the local standard deviation of thermal temperature were computed inside moving windows matched to the microwave support area. These variables summarize internal heterogeneity, row structure, thermal contrast, and exposed soil mixing. The retrieved feature set can be written as:

$$f = [FVC, T_{opt}, T_{tir}, H] \quad (2)$$

where FVC is the optical fraction vegetation cover, Topt denotes optical texture, Ttir denotes thermal texture, and H is a heterogeneity-related descriptor assembled from the footprint-scale statistics. Texture features were defined as local dispersion metrics computed over a footprint-matched neighborhood. For each sample location i, a spatial window Wi was extracted to match the effective microwave support, implemented as a heading-oriented ellipse (approximately 7 × 4 m) or, when disabled, a square approximation shown in Figure 3 (b).

Optical texture was computed from the luminance channel derived from RGB imagery (L=0.2989R+0.5870G+0.1140B) (ITU-R, 2012), while thermal texture was computed from the co-registered surface temperature field. The texture metrics were defined as the standard deviation within the footprint window.

Using the four calibration scenes, the feature vector f was mapped to a prior mean and prior uncertainty for τ:

https://doi.org/10.5194/egusphere-2026-2193
Preprint. Discussion started: 24 April 2026
© Author(s) 2026. CC BY 4.0 License.

$$\mu_{\tau,i} = \beta_0 + \beta_1 f_{c,i} \quad (3)$$

$$log\sigma_{\tau,i} = \gamma_0 + \gamma_1 H_i + \gamma_2 f_{c,i} \quad (4)$$

$$\sigma_{\tau,i} = clip[\exp(log\sigma_{\tau,i}), \sigma_{min}, \sigma_{max}] \quad (5)$$

Here, $f_{c,i}$ denotes the fraction vegetation cover and H_i is the footprint-scale heterogeneity descriptor. The coefficients β and γ were estimated from the calibration dataset. Calibration targets τ_i^* were obtained by inverting the τ–ω forward model using matched in situ soil moisture observations.

In the implementation, these scene-dependent estimates were stored as sample-wise variables and used together with auxiliary fields such as effective temperature, vegetation fraction, and heterogeneity level. Rather than assuming a universal τ prior, the method leverages high-resolution imagery to adapt both the expected attenuation level and its associated uncertainty to each microwave sample. The prior mean is primarily controlled by vegetation fraction, while the prior uncertainty is modeled through a log-linear function of heterogeneity and vegetation conditions. This strategy is consistent with previous findings that retrieval performance improves when passive microwave inversions are constrained by physically informed priors reflecting local vegetation state (Feldman et al., 2021; Barrée et al., 2021).

The posterior distribution is then defined as:

$$p(Ws, \tau \mid TB, f) \propto p(TB \mid Ws, \tau, T_g, \omega) \cdot p(\tau \mid f) \cdot p(Ws) \quad (6)$$

with a Gaussian likelihood:

$$p(TB \mid Ws, \tau, T_g, \omega) \propto e^{\left[\frac{-(TB_{obs} - TB_{mod})^2}{(2\sigma_{TB}{}^2)}\right]} \quad (7)$$

and a feature-informed prior:

$$\tau \mid f \sim N(\mu_\tau(f), \sigma_\tau{}^2(f)) \quad (8)$$

The soil moisture prior was weak and mainly used to keep the solution within the physically admissible range. Posterior inference was performed through Metropolis-Hastings sampling in the two-dimensional state space of (Ws, τ). Each chain was run for a fixed number of iterations (e.g., 1,000), with an initial burn-in period (e.g., 200 samples) discarded to reduce the influence of initial conditions. Convergence was assessed by inspecting the stability of posterior traces and ensuring that summary statistics (mean and variance) remained stable across the retained samples. The implementation stored posterior mean, posterior standard deviation, 95% credible interval bounds,

https://doi.org/10.5194/egusphere-2026-2193
Preprint. Discussion started: 24 April 2026
© Author(s) 2026. CC BY 4.0 License.

and entropy-like diagnostics for each retrieval.

2.5 Accuracy Evaluation and Baseline Comparison

Accuracy was evaluated using multiple statistical metrics, including root mean square error (RMSE), mean absolute error (MAE), and bias, to comprehensively assess both the magnitude and systematic deviation of the predictions.

The independent validation used experiments from six different scenes (~3.3 ha, 57 validation points), collected over two consecutive days (04/04/2026-05/04/2026), spanning pre- and post-rainfall conditions, with approximately three days of dry conditions preceding the first observation and a rainfall event occurring in the early hours of 05/04/2026. Calibration was performed exclusively on four scenes (~ 1.3 ha, 52 calibration points) in 03/04/2026, which makes the reported results a generalization test rather than a same-day fit. The calibration dataset included bare soil, garlic, and wheat fields, while the validation dataset included bare soil, garlic, rapeseed, wheat, maize, and lettuce fields.

The principal baseline was a Dobson plus dual-parameter τ–ω inversion without the RGB-TIR Bayesian prior. For the proposed method, 95% bootstrap confidence intervals were computed for the overall metrics to summarize uncertainty due to the finite validation sample.

Additional analyses were performed by land-cover class, by scene, by footprint representation, and by the relationship between texture and retrieval uncertainty.

3. Results

3.1 Retrieval performance under varying soil moisture conditions

The proposed Bayesian joint retrieval substantially improved independent validation performance relative to the baseline under relatively wet conditions on the first day after rainfall (05/04/2026), shown in Figure 4 (a). Across all 57 matched points, the proposed 4 m × 7 m ellipse configuration achieved RMSE = 0.0418 $m^3\ m^{-3}$, MAE = 0.0243 $m^3\ m^{-3}$, and bias = −0.0030 $m^3\ m^{-3}$. In contrast, the baseline produced RMSE = 0.0769 $m^3\ m^{-3}$, MAE = 0.0684 $m^3\ m^{-3}$, and bias = −0.0637 $m^3\ m^{-3}$. The bootstrap confidence intervals of the proposed solution were also compact, with RMSE = 0.0418 [0.0270, 0.0566] $m^3\ m^{-3}$ and MAE = 0.0243 [0.0163, 0.0336] $m^3\ m^{-3}$. Figure 4a shows that

https://doi.org/10.5194/egusphere-2026-2193
Preprint. Discussion started: 24 April 2026
© Author(s) 2026. CC BY 4.0 License.

the improvement is not limited to one metric. The proposed method reduced both absolute error and signed underestimation. The bias result is especially important because it indicates that the RGB–TIR prior pathway corrected the strong dry bias of the unconstrained tau–omega inversion instead of merely trading one error type for another.

A consistent improvement was also observed under relatively drier conditions on the day before rainfall (04/04/2026). In Figure 4 (b), the proposed method achieved RMSE = 0.038 $m^3 m^{-3}$, MAE = 0.023 $m^3 m^{-3}$, and bias = 0.004 $m^3 m^{-3}$, whereas the baseline yielded RMSE = 0.067 $m^3 m^{-3}$, MAE = 0.055 $m^3 m^{-3}$, and bias = −0.035 $m^3 m^{-3}$. The corresponding bootstrap confidence intervals for the proposed method remained compact, with RMSE = 0.038 [0.023, 0.054] $m^3 m^{-3}$ and MAE = 0.023 [0.015, 0.033] $m^3 m^{-3}$. Similar to the wetter case, the proposed approach substantially reduced both RMSE and MAE and brought the bias much closer to zero. Although the baseline still showed a clear negative bias under drier conditions, the proposed method largely removed this systematic underestimation. Taken together, Figure 4 demonstrates that the advantage of the Bayesian joint retrieval is robust across both relatively wet and relatively dry post-rainfall conditions, improving not only overall accuracy but also bias behavior across changing moisture regimes.

https://doi.org/10.5194/egusphere-2026-2193
Preprint. Discussion started: 24 April 2026
© Author(s) 2026. CC BY 4.0 License.

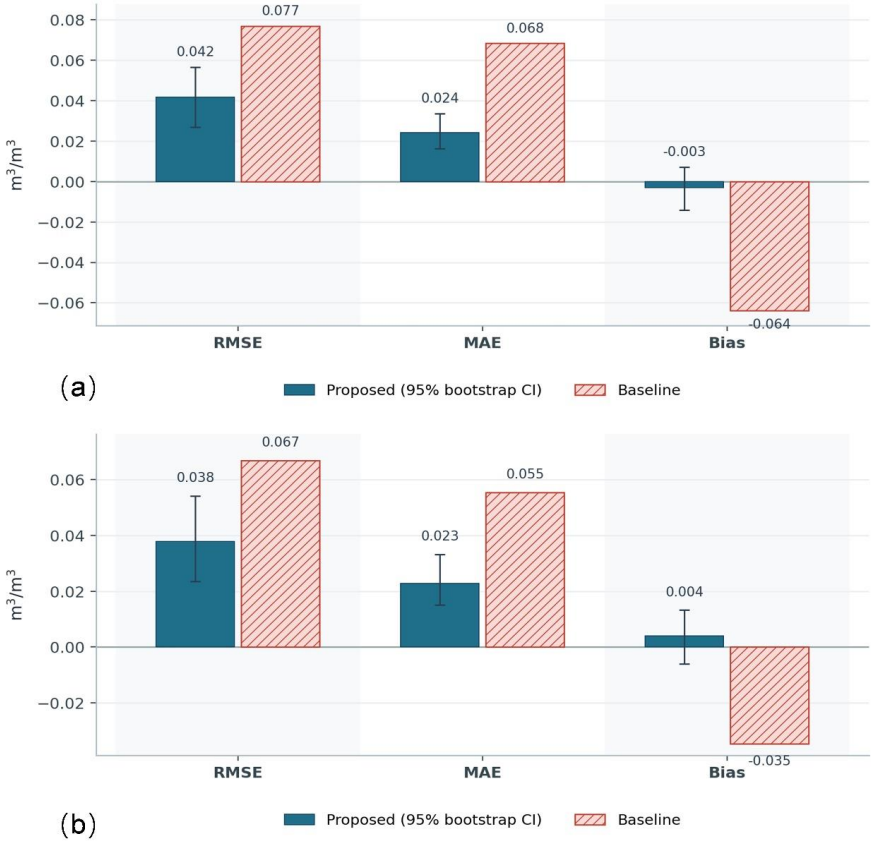

295 **Figure 4. Comparison of overall validation RMSE, MAE, and bias between the proposed Bayesian joint retrieval and the baseline inversion. Error bars denote the 95% bootstrap confidence interval for the proposed method. (a) Results on the day after rainfall (relatively wet) (05/04/2026), (b) Results on the day before rainfall (relatively dry) (04/04/2026).**

Figure 5 presents representative retrieval maps overlaid on the optical orthomosaics for two
300 moisture states, with panels (a-d) corresponding to the relatively drier conditions on 04/04 and panels (e-h) corresponding to the wetter conditions on 05/04 after the early-morning rainfall event. In both cases, the proposed retrieval preserves the broad field-scale soil moisture patterns while avoiding the pronounced dry shift evident in the baseline maps. Under the drier conditions, the proposed product maintains spatial gradients without collapsing toward unrealistically low values,
305 whereas under the wetter conditions it captures the overall increase in soil moisture while remaining coherent with field boundaries and within-field structure. The posterior estimates retain meaningful local variability while remaining within a physically plausible range supported by the auxiliary

https://doi.org/10.5194/egusphere-2026-2193
Preprint. Discussion started: 24 April 2026
© Author(s) 2026. CC BY 4.0 License.

optical and thermal information. In contrast, the baseline retrieval tends to drift toward overly dry values in both moisture states, especially where vegetation attenuation and temperature effects cannot be reliably separated from brightness temperature alone.

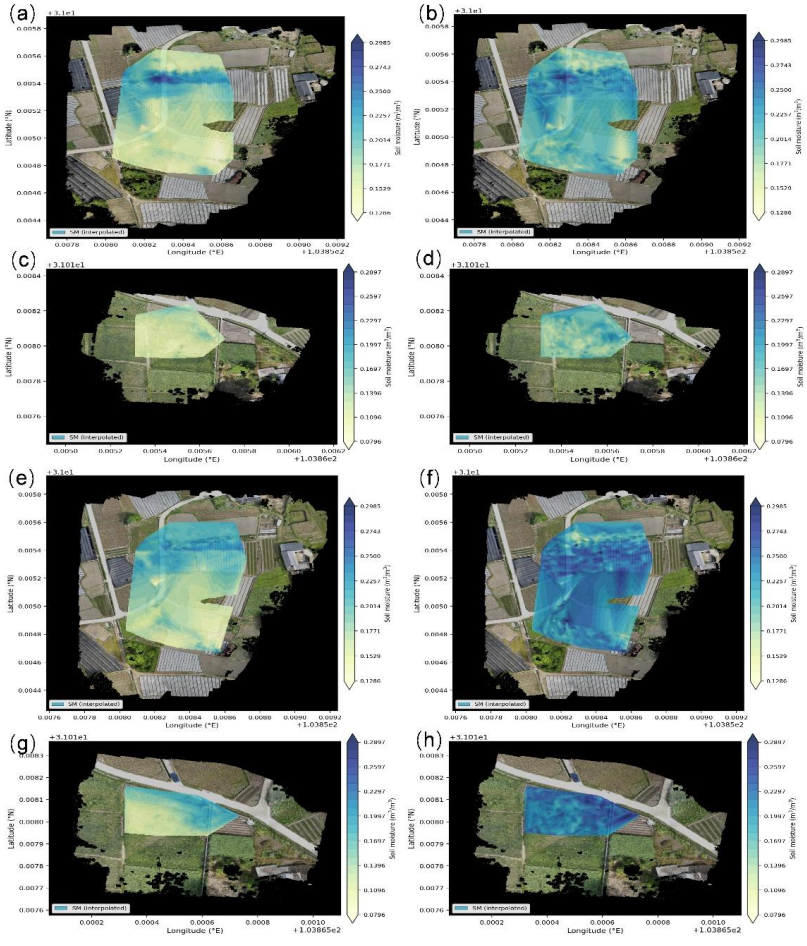

Figure 5. Representative soil moisture maps overlaid on optical orthomosaics. Panels (a-d) correspond to 04/04/2026 (relatively dry conditions) and panels (e-h) to 05/04/2026 (post-rainfall, relatively wet conditions). In each group, (a, c, e, g) show the baseline retrieval and (b, d, f, h) show the proposed Bayesian joint retrieval.

3.2 Retrieval performance under varying land cover

Land-cover stratification reveals that the gain of the proposed method was not uniform but remained positive across all categories represented in the validation set. Table 1 shows that the largest relative improvements occurred for wheat and maize, with RMSE decreasing from 0.0921 to 0.0088 $m^3 m^{-3}$

https://doi.org/10.5194/egusphere-2026-2193
Preprint. Discussion started: 24 April 2026
© Author(s) 2026. CC BY 4.0 License.

and from 0.0857 to 0.0187 $m^3 m^{-3}$, respectively. Bare soil also improved substantially (0.0507 to 0.0226 $m^3 m^{-3}$), while lettuce, garlic, and rapeseed (oilseed rape) showed more moderate but consistent gains. This consistent improvement across contrasting land-cover types indicates that the method is not exploiting crop-specific features, but rather provides a more stable attenuation constraint applicable across different surface conditions.

Table 1. Validation accuracy by land-cover type for the baseline retrieval and the proposed Bayesian joint retrieval

Type	Baseline			Bayesian joint retrieval		
	RMSE	MAE	Bias	RMSE	MAE	Bias
Bare soil	0.0507	0.0428	-0.0292	0.0226	0.0135	0.0098
Garlic	0.0844	0.0749	-0.0749	0.0692	0.0454	-0.0407
Wheat	0.0921	0.0889	-0.0889	0.0088	0.0068	0.0033
Lettuce	0.0757	0.0661	-0.0606	0.0500	0.0364	0.0146
Rapeseed	0.0797	0.0776	-0.0776	0.0396	0.0318	-0.0285
Maize	0.0857	0.0830	-0.0830	0.0187	0.0143	0.0143

Note: Values are reported in m3 m-3. Lower RMSE and MAE indicate better performance. Positive bias indicates wet overestimation.

A clear pattern is that the baseline retrieval exhibits a systematic negative bias across nearly all land-cover types, whereas the proposed method markedly reduces this dry bias and in some cases slightly overcorrects it. For example, wheat and maize biases shift from -0.0889 and -0.0830 $m^3 m^{-3}$ to values close to zero. This suggests that the unconstrained τ–ω inversion tends to over-attribute the signal to drier soil conditions, while the RGB-TIR-informed prior improves the partitioning between vegetation attenuation and soil emission.

The magnitude of improvement also varies with surface structure. Strong gains in wheat and maize likely reflect relatively uniform canopy conditions at the footprint scale, where prior constraints effectively reduce inversion ambiguity. Bare soil benefits mainly from reduced structural mismatch. In contrast, smaller improvements in lettuce, garlic, and rapeseed are consistent with more heterogeneous canopy-soil configurations, where sub-footprint mixing introduces representation error that cannot be fully resolved within the homogeneous τ–ω framework.

This pattern is also evident in Figure 5. In both the drier (04/04) and wetter (05/04) conditions, the baseline exhibits stronger dry shifts in areas with denser or more heterogeneous vegetation, whereas more uniform or bare surfaces show smaller distortions. The proposed method reduces these biases

https://doi.org/10.5194/egusphere-2026-2193
Preprint. Discussion started: 24 April 2026
© Author(s) 2026. CC BY 4.0 License.

across moisture states, but the magnitude of improvement remains dependent on canopy structure within the footprint, consistent with the class-based statistics in Table 1. This pattern suggests that retrieval performance is controlled by canopy structural homogeneity at the footprint scale.

4. Discussion

4.1 Sub-footprint heterogeneity and its role in soil moisture observation uncertainty

The uncertainty analysis highlights a key implication of footprint-scale observations: not all forms of sub-footprint heterogeneity contribute equally to the ambiguity of soil moisture retrieval. Figure 6 summarizes the relationships between optical and thermal texture metrics across different land-cover types and their associations with τ prior uncertainty, posterior retrieval uncertainty and absolute soil-moisture error.

Figure 6 shows that optical texture, quantified here as the standard deviation of optical luminance inside the assumed microwave footprint, had a clear and significant positive association with the posterior uncertainty of τ and with the absolute error of retrieved soil moisture. The relationship with τ uncertainty was moderate but significant (Spearman $\rho = 0.47$, $p = 0.0002$), and the relationship with |error| on soil moisture was similarly strong (Spearman $\rho = 0.46$, $p = 0.0003$). In contrast, the direct relationship between optical texture and posterior soil-moisture standard deviation was weak and not significant ($\rho = 0.09$, $p = 0.49$). Thermal texture showed weaker associations overall. It was significantly related to τ uncertainty ($\rho = 0.30$, $p = 0.023$), but not significantly related to posterior soil-moisture standard deviation or to absolute soil-moisture error. This pattern suggests that optical texture is the stronger indicator of internal structural mixing in the observed fields, while thermal texture is informative but more scene-dependent.

https://doi.org/10.5194/egusphere-2026-2193
Preprint. Discussion started: 24 April 2026
© Author(s) 2026. CC BY 4.0 License.

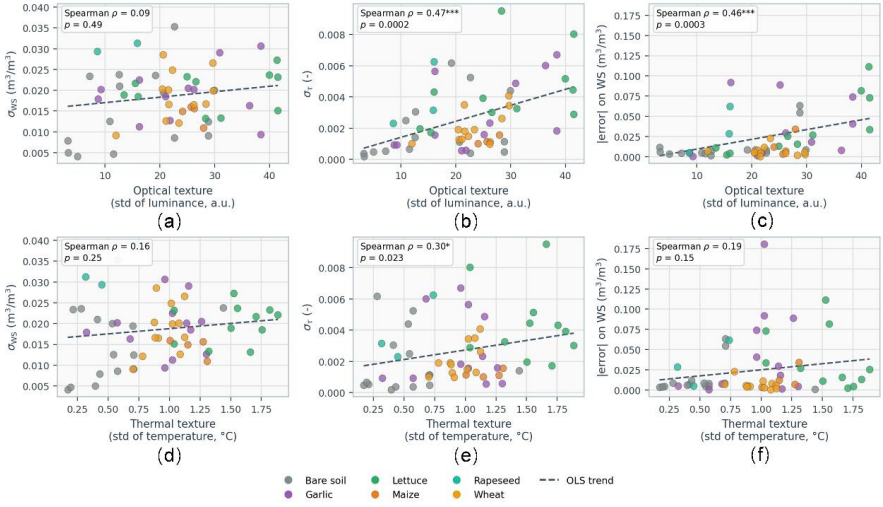

Figure 6. Relationships between footprint-scale optical and thermal texture and retrieval uncertainty. Panels (a)-(c) show optical texture versus posterior soil-moisture standard deviation, posterior tau uncertainty, and absolute soil-moisture error. Panels (d)-(f) show the corresponding thermal-texture relations.

These findings are physically plausible. The L-band radiometer measures an area-integrated brightness temperature over a footprint several meters wide. When the support area contains mixed canopy density, row structure, exposed soil patches, residue, or irrigation patterns, the measured brightness temperature becomes the nonlinear average of multiple sub-footprint states. In that situation, the inversion is asked to explain one aggregated microwave signal with one effective pair of soil moisture and vegetation optical depth. The solution therefore represents an equivalent state rather than a true point state. Because the τ–ω forward model is nonlinear, averaging before inversion is not equivalent to inversion before averaging. This Jensen-type effect is one of the reasons why heterogeneous scenes are intrinsically more difficult for passive microwave retrieval (Burke et al., 2003; Lakhankar et al., 2009; Chan et al., 2016). Recent L-band studies over heterogeneous scenes report similar behavior for the coupled retrieval of soil moisture and vegetation optical depth (Barrée et al., 2021; Feldman et al., 2021).

The present results refine the understanding of how sub-footprint heterogeneity affects soil moisture retrieval in two ways. First, they show that heterogeneity primarily enters the posterior through τ-related uncertainty rather than through a strong inflation of posterior soil-moisture variance. This

https://doi.org/10.5194/egusphere-2026-2193
Preprint. Discussion started: 24 April 2026
© Author(s) 2026. CC BY 4.0 License.

suggests that ambiguity in the microwave signal initially arises from vegetation attenuation and canopy–soil partitioning within the footprint, since τ directly controls the attenuation component in the tau–omega model. Different sub-footprint canopy arrangements can produce similar aggregate transmissivity, so the posterior of τ widens before the soil-moisture estimate becomes obviously unstable. Second, the fact that optical texture correlates more strongly with |error| than with σWs indicates that part of the representation error remains outside the posterior uncertainty term. In other words, while the inversion captures part of the ambiguity, the remaining error reflects structural mismatch between the real heterogeneous footprint and the homogeneous tau–omega representation. This distinction is important because it highlights that uncertainty estimates are informative for diagnosing retrieval ambiguity, but cannot fully substitute for improved physical representation of sub-footprint heterogeneity in hydrological observations.

The land-cover-specific results support the same interpretation. Lettuce fields show the strongest within-class relationship between optical texture and absolute error, consistent with the fine-scale canopy contrast and mixed exposed-soil structure visible in the orthomosaics, as lettuce is typically sparsely planted with interspersed bare soil and vegetation. Bare soil shows a weaker but still positive tendency, reflecting residual heterogeneity in surface conditions. In contrast, wheat exhibits only a weak within-class relation in the present sample, likely because the canopy structure is more spatially uniform at the scale of the radiometer footprint and because the prior pathway effectively constrains attenuation in these scenes. From a hydrological standpoint, this indicates that the role of "texture" is context-dependent rather than universal. Its influence depends on whether the high-resolution heterogeneity corresponds to physically meaningful contrasts in soil–vegetation structure that affect the L-band support area and the interpretation of soil moisture at the field scale.

The footprint experiment reinforces the mechanism argument. The 4 m × 7 m ellipse outperformed the 5 m × 5 m square even though both footprints covered similar total area. The most likely reason is not a change in total support size but a better match between the anisotropic radiometric support and the optical-thermal aggregation window. When the auxiliary priors are summarized over a shape that better approximates the actual microwave support, the resulting FVC and texture descriptors are more representative of what the radiometer "saw." This improves both the prior mean and the uncertainty term. It is evidence that physically consistent support matching matters when high-

https://doi.org/10.5194/egusphere-2026-2193
Preprint. Discussion started: 24 April 2026
© Author(s) 2026. CC BY 4.0 License.

resolution auxiliary data are injected into passive microwave retrieval.

Table 2. Comparison of retrieval accuracy between the physically matched 4 × 7 m ellipse footprint and a simplified 5 × 5 m square footprint

Footprint	RMSE	MAE	Bias
4*7 (Ellipse)	0.0418	0.0243	-0.0030
5*5 (Square)	0.0443	0.0291	0.0021

Note: The ellipse footprint better matches the field-estimated support area of the UAV L-band radiometer.

4.2 Sensitivity Analysis of Core Hyperparameters

The sensitivity analysis further shows that the proposed framework is not excessively fragile to moderate hyperparameter changes. Figure 7 summarizes one-at-a-time experiments for four key parameters: the microwave likelihood spread σTB, the scale applied to the τ prior mean, the prior-strength parameter κ, and the scale applied to the τ prior width. The resulting validation RMSE curves are relatively flat, and the spread of the error bars is larger than the change in the mean RMSE over much of the tested range. This indicates that the method is relatively stable once the prior pathway and support-matching strategy are in place.

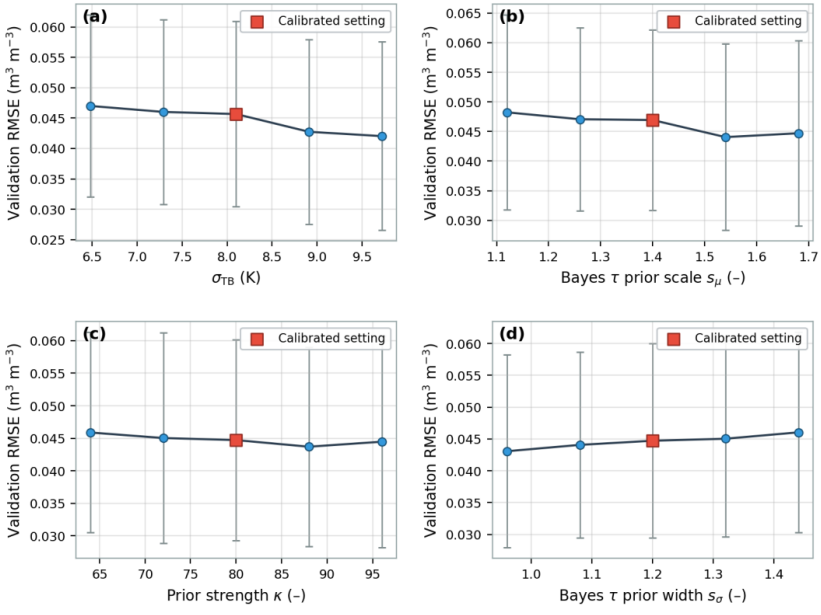

Figure 7. Sensitivity of validation RMSE to four key hyperparameters. The panels summarize one-at-a-time perturbations of the (a) microwave likelihood spread, (b) tau-prior mean scale, (c) prior strength, and (d) tau-

https://doi.org/10.5194/egusphere-2026-2193
Preprint. Discussion started: 24 April 2026
© Author(s) 2026. CC BY 4.0 License.

prior width; red squares indicate calibrated settings used in the sensitivity experiment.

The observed trends are nevertheless informative, as they consistently reflect the balance between fitting the microwave observations and enforcing physically meaningful prior constraints on soil moisture and vegetation attenuation. Increasing the effective likelihood spread from the lower tested values initially improved retrieval performance by preventing overfitting to noisy or structurally mismatched brightness temperatures, which can be interpreted as reducing the influence of representativeness error arising from sub-footprint heterogeneity. Similarly, moderate increases in the prior mean scale improved performance, indicating that the RGB-TIR-derived attenuation prior provides physically meaningful information on vegetation effects when appropriately weighted. The prior-strength experiment showed a clear monotonic improvement in RMSE until the curve flattened, suggesting that stronger prior control enhances retrieval stability by constraining physically unrealistic solutions, but only up to a point beyond which additional constraint limits the contribution of the microwave observations themselves. Consistent with previous findings in uncertainty-aware retrieval systems, physically meaningful regularization improves transferability as long as the prior does not overly constrain the solution and suppress observation-driven information (Karthikeyan et al., 2020; Konings et al., 2017). The width-scale experiment further supports this interpretation, showing a shallow optimum that confirms both under-confident and over-confident priors can lead to suboptimal representation of soil moisture under heterogeneous field conditions.

Taken together, these sensitivity experiments indicate that the calibrated parameter settings lie within a low-curvature region of the RMSE response surface. From a hydrological perspective, this suggests that the retrieval framework captures a stable balance between observation constraints and prior information across the tested conditions, rather than relying on narrowly tuned parameter values. Such behavior implies that the inferred soil moisture states are not highly sensitive to moderate perturbations in hyperparameters, which is important for maintaining physical consistency when transferring the method across fields with varying vegetation structure and surface conditions. This robustness is particularly relevant for field-scale hydrological applications, where calibration data are limited and environmental heterogeneity introduces unavoidable uncertainty.

https://doi.org/10.5194/egusphere-2026-2193
Preprint. Discussion started: 24 April 2026
© Author(s) 2026. CC BY 4.0 License.

4.3 Limitations and Future Directions

Several limitations remain. Although the independent validation was designed as a two-day repeated experiment (04/04-05/04) across six scenes per day and 57 matched points (~3.3 ha), providing a controlled test of short-term reproducibility under post-rainfall conditions, the overall sample size is still limited, and the results should be interpreted as indicative rather than definitive. The campaign represents a restricted set of dates and management conditions. While the calibration and validation scenes span multiple crops, they do not cover the full seasonal range of canopy development, irrigation dynamics, or surface roughness evolution. In particular, the validation focuses on two consecutive days following rainfall, capturing relatively wet and drier states but not longer-term temporal variability. Consequently, further validation across multiple seasons and broader environmental conditions is needed to fully assess the robustness and transferability of the proposed framework. The method should therefore be regarded as a well-supported field-scale prototype rather than a final universal model.

The RGB-TIR feature pathway can also be expanded. In the present study, optical and thermal information was summarized with simple and robust descriptors, especially fraction vegetation cover and local texture statistics. These descriptors worked well, but they do not fully represent canopy architecture, row orientation, spectral variability, or directional effects. More advanced optical or thermal descriptors, and additional multispectral or hyperspectral channels, could help to further separate canopy effects from soil-background effects. This direction is supported by recent optical-thermal soil moisture studies that obtained additional gains when canopy context was described more explicitly (Sahaar et al., 2022; Shi et al., 2024; Vahidi et al., 2025).

Another useful extension would be broader uncertainty partitioning. The present framework quantifies posterior uncertainty conditioned on the chosen forward model and prior pathway, but it does not separately decompose measurement noise, co-registration error, and model structural error. Future work could combine the current Bayesian retrieval with hierarchical error models, alternative support representations, or explicit assimilation strategies. Related recent studies in Bayesian remote sensing and hydrologic inversion indicate that this is a promising pathway for improving both interpretability and operational confidence (Jing et al., 2025).

https://doi.org/10.5194/egusphere-2026-2193
Preprint. Discussion started: 24 April 2026
© Author(s) 2026. CC BY 4.0 License.

5. Conclusion

This study developed a Bayesian joint retrieval framework for UAV-based L-band soil moisture estimation that integrates RGB and thermal infrared information through physically consistent, footprint-scale priors. The results highlight that field-scale soil moisture retrieval is fundamentally constrained by sub-footprint heterogeneity and observation support mismatch.

Three main conclusions can be drawn.

(1) Incorporating RGB-TIR-informed priors significantly improved retrieval performance and reduced the systematic dry bias of the conventional τ–ω inversion, demonstrating the value of physically constrained auxiliary information.

(2) Sub-footprint heterogeneity was identified as a key source of retrieval ambiguity, primarily affecting vegetation attenuation (τ) uncertainty and canopy-soil partitioning rather than directly destabilizing soil moisture estimates. This indicates that representation error plays a central role in field-scale soil moisture observation.

(3) Physically consistent support matching, implemented through an ellipse-shaped footprint, improved retrieval performance, emphasizing that the integration of multi-source data must respect the actual observation scale of microwave measurements.

Overall, the findings suggest that improving soil moisture retrieval is not only a matter of algorithm design, but also of better representing the relationship between observation scale, surface heterogeneity, and physical processes. This has direct implications that rely on spatially representative soil moisture, including infiltration estimation, land–atmosphere exchange, and field-scale water management.

The current results are based on a limited number of scenes and short-term observations, and further evaluation across broader environmental conditions is required to assess the generality of the proposed framework.

Acknowledgments

This study has been supported by the National Natural Science Foundation of China (U2442201 & 523B1006 & 52309024), and Fujian Key Laboratory of Severe Weather & Key Laboratory of Straits

https://doi.org/10.5194/egusphere-2026-2193
Preprint. Discussion started: 24 April 2026
© Author(s) 2026. CC BY 4.0 License.

Severe Weather, China Meteorological Administration (2024KFKT02).

Data Available Statement

The running python codes are available at Zenodo (Li, 2026).

Author contributions

ZL: Conceptualization; Data curation; Model development; Investigation; Methodology; Validation; Visualization; Writing – original draft; Writing – review & editing.

YL: Conceptualization; Investigation; Methodology; Writing – review & editing

RT: Conceptualization; Funding acquisition; Investigation; Methodology; Supervision; Writing – review & editing.

PC: Investigation; Methodology; Writing – review & editing.

FT: Funding acquisition; Methodology; Supervision; Writing – review & editing.

YZ: Investigation; Validation; Writing – review & editing.

Competing interests

At least one of the (co-)authors is a member of the editorial board of Hydrology and Earth System Sciences. The authors also have no other competing interests to declare.

References

Alburn, N. E., Niemann, J. D., and Elhaddad, A.: Evaluation of a surface energy balance method based on optical and thermal satellite imagery to estimate root-zone soil moisture, Hydrol. Process., 29, 5354–5368, 2015.

Barrée, M., Mialon, A., Pellarin, T., Parrens, M., Biron, R., Lemaître, F., Gascoin, S., and Kerr, Y.: Soil moisture and vegetation optical depth retrievals over heterogeneous scenes using LEWIS L-band radiometer, Int. J. Appl. Earth Obs. Geoinf., 102, 102424, https://doi.org/10.1016/j.jag.2021.102424, 2021.

Burke, E. J. and Simmonds, L. P.: Effects of sub-pixel heterogeneity on the retrieval of soil moisture from passive microwave radiometry, Int. J. Remote Sens., 24, 2085–2104, https://doi.org/10.1080/01431160210155938, 2003.

https://doi.org/10.5194/egusphere-2026-2193
Preprint. Discussion started: 24 April 2026
© Author(s) 2026. CC BY 4.0 License.

Chan, S. K., Bindlish, R., O'Neill, P. E., Jackson, T. J., Njoku, E. G., and Dunbar, R. S.: Assessment of the SMAP passive soil moisture product, IEEE T. Geosci. Remote, 54, 4994–5007, 2016.

Dobson, M., Ulaby, F., Hallikainen, M., and El-Rayes, M.: Microwave dielectric behavior of wet soil – Part II: Dielectric mixing models, IEEE T. Geosci. Remote, GE-23, 35–46, https://doi.org/10.1109/TGRS.1985.289498, 1985.

Ebtehaj, A. and Bras, R. L.: A physically constrained inversion for high-resolution passive microwave retrieval of soil moisture and vegetation water content in L-band, Remote Sens. Environ., 233, 111346, https://doi.org/10.1016/j.rse.2019.111346, 2019.

Escorihuela, M., Chanzy, A., Wigneron, J., and Kerr, Y.: Effective soil moisture sampling depth of L-band radiometry: A case study, Remote Sens. Environ., 114, 995–1001, https://doi.org/10.1016/j.rse.2009.12.011, 2010.

Feldman, A., Chaparro, D., and Entekhabi, D.: Error propagation in microwave soil moisture and vegetation optical depth retrievals, IEEE J. Sel. Top. Appl., 14, 11311–11323, https://doi.org/10.1109/JSTARS.2021.3124857, 2021.

Gao, Y., Lian, X., and Ge, L.: Inversion model of surface bare soil temperature and water content based on UAV thermal infrared remote sensing, Infrared Phys. Techn., 125, 104289, https://doi.org/10.1016/j.infrared.2022.104289, 2022.

Gibon, F., Mialon, A., Richaume, P., Rodríguez-Fernández, N., Aberer, D., Boresch, A., Crapolicchio, R., Dorigo, W., Gruber, A., Himmelbauer, I., Preimesberger, W., Sabia, R., Stradiotti, P., Tercjak, M., and Kerr, Y. H.: Estimating the uncertainties of satellite derived soil moisture at global scale, Sci. Remote Sens., 10, 100147, https://doi.org/10.1016/j.srs.2024.100147, 2024.

Gruber, A., De Lannoy, G., Albergel, C., Al-Yaari, A., Brocca, L., Calvet, J. C., Colliander, A., Cosh, M., Crow, W., Dorigo, W., Draper, C., Hirschi, M., Kerr, Y., Konings, A., Lahoz, W., McColl, K., Montzka, C., Muñoz-Sabater, J., Peng, J., and Reichle, R.: Validation practices for satellite soil moisture retrievals: What are (the) errors?, Remote Sens. Environ., 244, 111806, https://doi.org/10.1016/j.rse.2020.111806, 2020.

Houtz, D., Naderpour, R., and Schwank, M.: Portable L-band radiometer (PoLRa): Design and characterization, Remote Sens., 12, 2780, https://doi.org/10.3390/rs12172780, 2020.

International Telecommunication Union: Recommendation ITU-R BT.601-7: Studio encoding parameters of digital television for standard 4:3 and wide-screen 16:9 aspect ratios, International Telecommunication Union, 2012.

Jääskeläinen, E., Luoto, M., Putkiranta, P., Aurela, M., and Virtanen, T.: High-resolution soil moisture mapping in northern boreal forests using SMAP data and downscaling techniques, Hydrol. Earth Syst. Sci., 29, 6237–6256, 2025.

Jing, H., Chai, L., Liu, S., Chen, D., Zhao, S., and Zhu, Z.: Improve the accuracy of SAR-based

https://doi.org/10.5194/egusphere-2026-2193
Preprint. Discussion started: 24 April 2026
© Author(s) 2026. CC BY 4.0 License.

soil moisture retrieval by coupling Bayesian inference and water cloud model, J. Hydrol., 666, 134826, https://doi.org/10.1016/j.jhydrol.2025.134826, 2025.

Karthikeyan, L., Pan, M., Kumar, D. N., and Wood, E. F.: Effect of structural uncertainty in passive microwave soil moisture retrieval algorithm, Sensors, 20, 1225, 2020.

Kerr, Y. H., Waldteufel, P., Wigneron, J. P., Delwart, S., Cabot, F., Boutin, J., Escorihuela, M. J., Font, J., Reul, N., Gruhier, C., Juglea, S. E., Drinkwater, M. R., Hahne, A., Martín-Neira, M., and Mecklenburg, S.: The SMOS mission: New tool for monitoring key elements of the global water cycle, Proc. IEEE, 98, 666–687, https://doi.org/10.1109/JPROC.2010.2043032, 2010.

Konings, A. G., Piles, M., Rötzer, K., McColl, K. A., Chan, S. K., and Entekhabi, D.: Vegetation optical depth and scattering albedo retrieval using time series of dual-polarized L-band radiometer observations, Remote Sens. Environ., 193, 231–242, 2017.

Krishnan, S., Nair, A. S., Indu, J., Jove-Casulleras, R., and Gonzalvez-Foguet, R.: Brightness temperature and emissivity retrieved from a portable L-band radiometer, Int. J. Remote Sens., 43, 2503–2516, https://doi.org/10.1080/01431161.2022.2063039, 2022.

Krishnan, S. and Indu, J.: Evaluating soil moisture retrieved from a portable L-band radiometer, Adv. Space Res., 75, 2018–2027, https://doi.org/10.1016/j.asr.2024.10.049, 2025.

Lakhankar, T., Ghedira, H., Temimi, M., Azar, A. E., and Khanbilvardi, R.: Effect of land cover heterogeneity on soil moisture retrieval using active microwave remote sensing data, Remote Sens., 1, 80–91, https://doi.org/10.3390/rs1020080, 2009.

Li, W., Liu, C., Yang, Y., Awais, M., Li, W., Ying, P., Ru, W., and Cheema, M. J. M.: A UAV-aided prediction system of soil moisture content relying on thermal infrared remote sensing, Int. J. Environ. Sci. Te., 19, 9587–9600, https://doi.org/10.1007/s13762-022-03958-7, 2022.

Li, W., Migliavacca, M., Forkel, M., Denissen, J. M. C., Reichstein, M., Yang, H., Duveiller, G., Weber, U., and Orth, R.: Widespread increasing vegetation sensitivity to soil moisture, Nat. Commun., 13, 3959, 2022.

Li, Y., Yan, S., and Gong, J.: Quantifying uncertainty in soil moisture retrieval using a Bayesian neural network framework, Comput. Electron. Agr., 215, 108414, https://doi.org/10.1016/j.compag.2023.108414, 2023.

Li, Z.: The open code of paper titled "Bayesian joint retrieval of soil moisture from UAV L-band radiometry by integrating RGB-TIR priors and footprint-scale texture", Zenodo, https://doi.org/10.5281/zenodo.19587715, 2026.

Lu, Z., Fan, L., Liu, X., Bai, X., Baghdadi, N., Frappart, F., Zeng, J., De Lannoy, G., Peng, J., Xing, Z., Li, X., Feng, Z., Li, X., and Wigneron, J. P.: Sentinel-1 vegetation optical depth retrievals over the international soil moisture network, Int. J. Digit. Earth, 18, 2555412, https://doi.org/10.1080/17538947.2025.2555412, 2025.

Lv, S., Houtz, D., Li, S., Hu, Y., Zhang, J., Wu, D., Jin, L., and Wen, J.: Rapid retrieval of soil

https://doi.org/10.5194/egusphere-2026-2193
Preprint. Discussion started: 24 April 2026
© Author(s) 2026. CC BY 4.0 License.

moisture using a novel portable L-band radiometer in the Hulunbeier Prairie, China, GISci. Remote Sens., 61, 2424337, https://doi.org/10.1080/15481603.2024.2424337, 2024.

Messina, G. and Modica, G.: Applications of UAV thermal imagery in precision agriculture: State of the art and future research outlook, Remote Sens., 12, 1491, https://doi.org/10.3390/rs12091491, 2020.

Meyer, G. E. and Neto, J. C.: Verification of color vegetation indices for automated crop imaging applications, Comput. Electron. Agr., 63, 282–293, 2008.

Meyer, R., Zhang, W., Kragh, S. J., Andreasen, M., Jensen, K. H., Fensholt, R., and Looms, M. C.: Exploring the combined use of SMAP and Sentinel-1 data for downscaling soil moisture beyond the 1 km scale, Hydrol. Earth Syst. Sci., 26, 3337–3357, 2022.

Peng, J., Loew, A., Merlin, O., and Verhoest, N.: A review of spatial downscaling of satellite remotely sensed soil moisture, Rev. Geophys., 61, e2021RG000765, 2023.

Sahaar, S. A., Niemann, J. D., and Elhaddad, A.: Using regional characteristics to improve uncalibrated estimation of rootzone soil moisture from optical/thermal remote-sensing, Remote Sens. Environ., 273, 112982, https://doi.org/10.1016/j.rse.2022.112982, 2022.

Shen, X., Walker, J. P., Ye, N., Wu, X., Boopathi, N., Yeo, I. Y., Zhang, L., and Zhu, L.: Soil moisture retrieval depth of P- and L-band radiometry: Predictions and observations, IEEE T. Geosci. Remote, 59, 6814–6822, https://doi.org/10.1109/TGRS.2020.3026384, 2021.

Shi, H., Liu, Z., Li, S., Jin, M., Tang, Z., Sun, T., Liu, X., Li, Z., Zhang, F., and Xiang, Y.: Monitoring soybean soil moisture content based on UAV multispectral and thermal-infrared remote-sensing information fusion, Plants, 13, 2417, https://doi.org/10.3390/plants13172417, 2024.

Su, S. L., Singh, D. N., and Baghini, M. S.: A critical review of soil moisture measurement, Measurement, 54, 92–105, 2014.

Vahidi, M., Shafian, S., and Frame, W. H.: Depth-specific soil moisture estimation in vegetated corn fields using a canopy-informed model: A fusion of RGB-thermal drone data and machine learning, Agr. Water Manage., 307, 109213, https://doi.org/10.1016/j.agwat.2024.109213, 2025.

Wang, W., Ma, C., Wang, X., Feng, J., Dong, L., Kang, J., Jin, R., and Li, X.: A soil moisture experiment for validating high-resolution satellite products and monitoring irrigation at agricultural field scale, Agr. Water Manage., 304, 109071, https://doi.org/10.1016/j.agwat.2024.109071, 2024.

Wang, Y., Shi, L., Hu, Y., Hu, X., Song, W., and Wang, L.: A comprehensive study of deep learning for soil moisture prediction, Hydrol. Earth Syst. Sci. Discuss., 2023, 1–38, 2023.

Wigneron, J. P., Kerr, Y., Waldteufel, P., Saleh, K., Escorihuela, M. J., Richaume, P., Ferrazzoli, P., de Rosnay, P., Gurney, R., Calvet, J. C., Grant, J., Guglielmetti, M., Hornbuckle, B., Mätzler, C., Pellarin, T., and Schwank, M.: L-band microwave emission of the biosphere (L-MEB)

https://doi.org/10.5194/egusphere-2026-2193
Preprint. Discussion started: 24 April 2026
© Author(s) 2026. CC BY 4.0 License.

model: Description and calibration against experimental data sets over crop fields, Remote Sens. Environ., 107, 639–655, https://doi.org/10.1016/j.rse.2006.10.014, 2007.

Zhang, R., Nayak, A., Houtz, D., Watts, A., Soltanaghai, E., and Alipour, M.: Evaluation of soil moisture retrievals from a portable L-band microwave radiometer, Remote Sens., 16, 4596, https://doi.org/10.3390/rs16234596, 2024.

Zhao, T., Shi, J., Entekhabi, D., Jackson, T. J., Hu, L., Peng, Z., Yao, P., Li, S., and Kang, C. S.: Retrievals of soil moisture and vegetation optical depth using a multi-channel collaborative algorithm, Remote Sens. Environ., 257, 112321, https://doi.org/10.1016/j.rse.2021.112321, 2021.